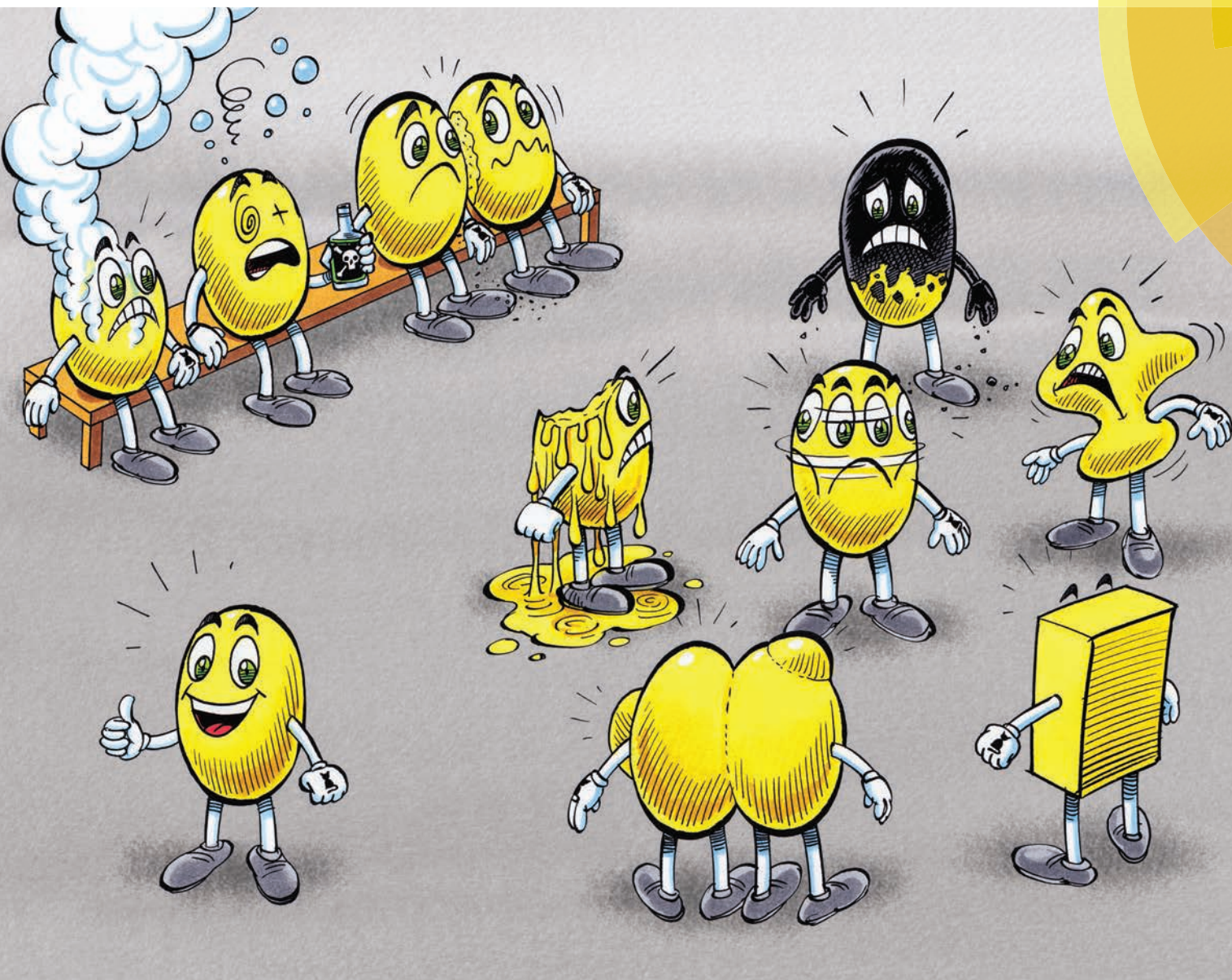


# Green Chemistry

Cutting-edge research for a greener sustainable future

[www.rsc.org/greenchem](http://www.rsc.org/greenchem)



ISSN 1463-9262



PAPER

C. Mondelli, J. Pérez-Ramírez *et al.*

Deactivation mechanisms of tin-zeolites in biomass conversions

**175** YEARS



Cite this: *Green Chem.*, 2016, **18**, 1249

## Deactivation mechanisms of tin-zeolites in biomass conversions†

G. M. Lari, P. Y. Dapsens, D. Scholz, S. Mitchell, C. Mondelli\* and J. Pérez-Ramírez\*

Metal-containing zeolites comprise outstandingly active and selective catalysts for a multitude of Lewis-acid and redox catalysed reactions that valorise renewable substrates into chemicals. Herein, focussing on tin-zeolites applied to the isomerisation of dihydroxyacetone (DHA) and xylose, we systematically study the influence of the framework type (MFI, MOR, BEA and FAU), preparation method (hydrothermal synthesis or alkaline-assisted metallation), hydrophobicity and nature of the solvent (water or methanol) on their intrinsic activity and, especially, on their stability. BEA and FAU zeolites were more active than MFI and MOR stannosilicates in aqueous and, particularly, in methanol-based tests owing to the larger relative amount of tetrahedral tin sites and/or superior mass transfer properties. Hydrothermally-prepared zeolites generally exhibited higher turnover frequencies than those obtained by a post-synthetic approach in view of their higher tin quality and less hydrophilic character. Remarkably, continuous-flow tests in a fixed-bed reactor indicated that exposure to reaction conditions for 24 hours could provoke dramatic changes in performance. Mainly due to amorphisation and modification of the tin structure (from tetra- to hexacoordination), the activity and selectivity of MOR, BEA and FAU zeolites were substantially, if not fully, depleted in the aqueous isomerisation of DHA, while MFI zeolites, especially the post-synthetically stannated sample, better preserved their initial performance. These deactivation phenomena were alleviated through the use of methanol, an industrially more amenable solvent, but, due to the greater retention of activity, fouling was more pronounced, particularly for MFI zeolites. In contrast, more extensive metal leaching was detected owing to the higher solubility of tin in the alcohol rather than water, where it hydrolyses into insoluble hydroxide species. In xylose isomerisation, hydrothermally-prepared MFI and BEA stannosilicates displayed reasonably stable operation. Deactivation mechanisms partly resembled those of the aqueous DHA isomerisation, but the chelating properties of the substrate played a greater detrimental role in tin loss.

Received 10th September 2015,  
Accepted 2nd November 2015

DOI: 10.1039/c5gc02147b

www.rsc.org/greenchem

## Introduction

Heterogeneous catalysis comprises a highly instrumental tool toward the production of added-value chemicals through the valorisation of biobased feedstocks.<sup>1</sup> Thanks to their tuneable redox and acidic properties, zeolites have demonstrated outstanding versatility.<sup>2</sup> Most prominently, transition metal-containing zeolites have been successfully applied to a variety of oxidations and of Lewis-acid catalysed isomerisation, cycloaddition and retro-aldol reactions.<sup>3</sup> The introduction of Sn,

Ga, Ti and Zr, mainly, into high-silica matrices has been achieved *via* distinct approaches.<sup>4</sup> In this respect, hydrothermal synthesis has played a foremost role till concerns about its scalability were raised in relationship to the most performing and studied material, *i.e.*, Sn-beta, which can only be crystallised in the presence of fluoride ions. Thus, more industrially-viable methods have been recently developed based on the post-synthetic metallation of commercial zeolites, using facile dry or wet procedures involving non-toxic reactants and yielding active materials.<sup>5</sup> Still, in view of a prospective industrial implementation, information about the long-term stability of these solids under reaction conditions is lacking.<sup>4,6</sup> Since the highly oxygenated and thermally unstable bio-derived substrates have to be converted in water or polar organics at temperatures generally in the range of 373 to 473 K, additional deactivation modes are expected compared to those commonly observed for the gas-phase conversion of hydrocarbons.<sup>1,7</sup> Besides poisoning or blocking of active sites by deposition of reactants, (by-)products and coke, competitive

*Institute for Chemical and Bioengineering, Department of Chemistry and Applied Biosciences, ETH Zurich, Vladimir-Prelog-Weg 1, CH-8093 Zurich, Switzerland.*

*E-mail: cecilia.mondelli@chem.ethz.ch, jpr@chem.ethz.ch; Fax: +41 44 6331405;*

*Tel: +41 44 6337120*

† Electronic supplementary information (ESI) available: Initial conversion and selectivity data for the continuous reactions over all zeolites and selectivity *vs.* time-on-stream for the continuous reactions over Sn-MFI. See DOI: 10.1039/c5gc02147b

adsorption of the solvent on the Lewis-acid sites or solvolysis of metal–oxygen bonds can occur leading to a restructuring of the active centre.<sup>8</sup> This eases its expulsion from the framework promoting the formation of leached species in the reaction medium, which may homogeneously contribute to the process.<sup>9</sup> In the case of less robust frameworks (*e.g.*, FAU) or of materials rich in surface defects, water can even cleave the zeolitic bonds under hydrothermal conditions causing the amorphisation of the structure.<sup>10</sup>

Most of the authors who assessed the stability of metal-containing zeolites in the liquid-phase conversion of biomass performed a repetition of batch experiments. Since these tests have typically been conducted at full conversion, limited insights into the extent and kinetics of deactivation have been gained so far. Exceptionally, reliable indications have been gathered for [Sn]BEA applied to the isomerisation of glucose.<sup>6,11</sup> However, continuous-flow testing in a fixed-bed reactor should be preferred to the batch protocol since it is an industrially more relevant operation mode and enables the exclusion of the role of homogeneous catalysis by possibly leached species in a direct manner. This has been applied only in a few studies which explored the use of [Sn]BEA for C–C coupling or [Sn]BEA and [Hf]BEA for transfer hydrogenation reactions.<sup>12</sup>

Herein, we studied tin-containing MFI, MOR, BEA and FAU zeolites prepared by hydrothermal synthesis in the presence of hydroxide or fluoride ions and/or alkaline-assisted metallation in the conversion of dihydroxyacetone and pyruvaldehyde into lactic acid and methyl lactate and of xylose into xylulose (Scheme 1). After evaluating their intrinsic activities in batch tests performed at low conversion, we assessed their stability through continuous-flow measurements. In-depth characteris-

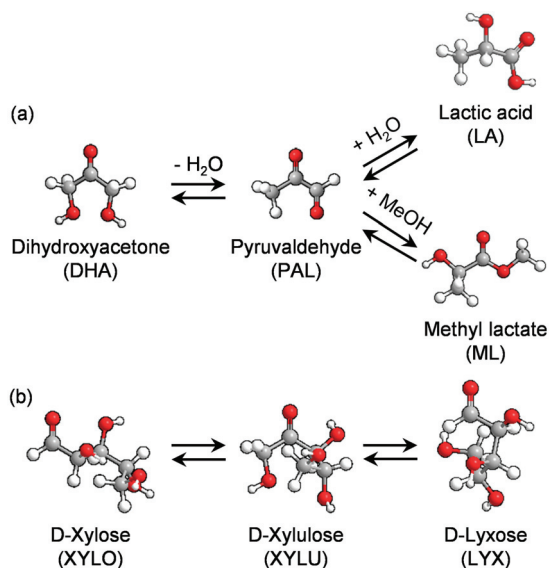
ation of the fresh and used catalysts sheds light on the role of the framework type, the preparation method, the hydrophobicity, the nature of the solvent and of the substrate on the deactivation behaviour.

## Experimental

### Catalyst synthesis

**Hydrothermal synthesis of [Sn]MFI.** Sn-containing zeolites with MFI framework topology were prepared by hydrothermal synthesis in the presence of OH<sup>−</sup> or F<sup>−</sup> ions as mineralising agents following the protocols reported by Mal *et al.*<sup>13</sup> In the first case, tetraethyl orthosilicate (TEOS, 93.5 g, Sigma-Aldrich, 98%) was added to a solution of SnCl<sub>4</sub>·5H<sub>2</sub>O (1.27 g, Sigma-Aldrich, 98%) in deionised H<sub>2</sub>O (29.9 g) and the mixture was stirred for 30 min. Then, tetrapropylammonium hydroxide (TPAOH, 198 g, Alfa Aesar, 20 wt%) was added dropwise and the mixture was stirred for another hour. Finally, 84 g of deionised H<sub>2</sub>O were added and the stirring was continued for 30 min. The final sol (0.008SnO<sub>2</sub> : 1SiO<sub>2</sub> : 0.44TPAOH : 31.5H<sub>2</sub>O on mole basis) was transferred into a 500 cm<sup>3</sup> Teflon-lined autoclave and heated at 433 K for 3 days under static conditions. In the second preparation, a solution of SnCl<sub>4</sub>·5H<sub>2</sub>O (1.25 g) in deionised H<sub>2</sub>O (50 g) was added dropwise and under rapid stirring to a solution of NH<sub>4</sub>F (26.75 g, Acros, 98%) in deionised H<sub>2</sub>O (125 g). Thereafter, a solution of tetrapropylammonium bromide (TPABr, 49 g, ABCR, 98%) in deionised H<sub>2</sub>O (280 g) was slowly added to the mixture, which was then stirred for 30 min. Finally, 43 g of fumed silica (Sigma-Aldrich) were added and the resulting sol (0.005SnO<sub>2</sub> : 1SiO<sub>2</sub> : 0.26TPAOH : 1NH<sub>4</sub>F : 35H<sub>2</sub>O on mole basis) was stirred for 3 h. The sol was then transferred into a 500 cm<sup>3</sup> Teflon-lined autoclave and heated at 473 K for 6 days under static conditions. The [Sn]MFI crystals resulting from the two procedures were separated by filtration, washed thoroughly with deionised water, dried overnight at 338 K and calcined in static air at 823 K (5 K min<sup>−1</sup>) for 5 h to ensure the complete removal of the organic structure directing agent. Subsequently, the two materials were ion exchanged in a 0.1 M aqueous NH<sub>4</sub>NO<sub>3</sub> solution (6 h, 298 K, 100 cm<sup>3</sup> per gram of dried zeolite, 3 times) followed by calcination under the conditions mentioned above. This procedure was applied to remove sodium from the solid obtained by the hydroxide route and performed over the fluoride-derived zeolite too for the sake of consistency. The two zeolites were labelled as [Sn]MFI-OH and [Sn]MFI-F, respectively.

**Hydrothermal synthesis of [Sn]BEA.** A tin-containing zeolite with BEA topology was prepared following the method reported by Corma *et al.*<sup>14</sup> Briefly, 30 g of TEOS and 33 g of tetraethylammonium hydroxide (Sigma-Aldrich, 35 wt%) were mixed for 90 min. Thereafter, a solution of 0.45 g SnCl<sub>4</sub>·5H<sub>2</sub>O in water (2.75 cm<sup>3</sup>) was added and the stirring was continued until complete evaporation of the ethanol formed upon hydrolysis. Then, 3.2 g of HF (Sigma-Aldrich, 48%) were added to the clear solution under stirring, resulting in the formation of a thick gel. Finally, a suspension of 0.36 g of commercial



**Scheme 1** Reaction network for the isomerisation of (a) dihydroxyacetone and (b) xylose.

zeolite beta (Tosoh Corporation, bulk Si/Al = 220) in water (2.75 cm<sup>3</sup>) was added and the gel was transferred into a 100 cm<sup>3</sup> Teflon-lined autoclave and heated at 413 K for 11 days. Thereafter, the solid was subjected to the same filtration, calcination and ion exchange procedures as described above. The final material was labelled as [Sn]BEA-F.

**Alkaline-assisted stannation of MFI, MOR, BEA and FAU zeolites.** MFI (Tosoh Corp., bulk Si/Al = 940), MOR (Tosoh Corp., bulk Si/Al = 110), BEA (Tosoh Corp., bulk Si/Al = 220) and FAU (Zeolyst, bulk Si/Al = 405) zeolites were used as received for the post-synthetic incorporation of tin. The zeolite (6.6 g in the case of MFI, 26.6 g for MOR, FAU and BEA) was added to an aqueous solution of NaOH (0.3 M, 100 cm<sup>3</sup>) and SnSO<sub>4</sub> (0.04 M) and the mixture was stirred at 338 K for 30 min in an Easymax™ 102 reactor system (Mettler Toledo). In the case of FAU and BEA, TPAOH (0.2 M) was added to the solution to minimise alterations in their crystallinity.<sup>15</sup> Thereafter, the treatment was quenched in 2 dm<sup>3</sup> distilled water and the suspended material filtered and washed until neutral pH of the filtrate was achieved. Calcination and ion exchange were performed on these solids following the same protocols as detailed above. These zeolites were labelled as Sn-MFI, Sn-MOR, Sn-BEA and Sn-FAU.

### Catalyst characterisation

The Si and Sn contents in the samples were determined by inductively coupled plasma optical emission spectroscopy (ICP-OES) using a Horiba Ultra 2 instrument equipped with a photomultiplier tube detector. Powder X-ray diffraction (XRD) was performed using a PANalytical X'Pert PRO-MPD diffractometer with Ni-filtered Cu K $\alpha$  radiation ( $\lambda = 0.1541$  nm), acquiring data in the 5–70° 2 $\theta$  range with a step size of 0.05° and a counting time of 8 s per step. The crystallinity was estimated from the ratio between the area of selected reflections of the used and fresh samples. The following peaks were used: 2 $\theta = 23.10^\circ$ , 23.95° and 24.42° for MFI, 2 $\theta = 25.82^\circ$  and 26.55° for MOR, 2 $\theta = 22.55^\circ$  for BEA and 2 $\theta = 15.85^\circ$  for FAU. N<sub>2</sub> sorption at 77 K was conducted using a Micromeritics TriStar analyser. Prior to the measurements, the samples were degassed at 573 K under vacuum for 3 h. UV-Vis spectroscopy was carried out in diffuse reflectance mode using an Ocean Optics Maya2000-Pro spectrometer. Prior to the analyses, samples were degassed at 313 K under vacuum for 16 h. Spectra were collected in Kubelka–Munk (KM) units in the 200–600 nm range, with an integration time of 150 ms and accumulating 32 scans. They were corrected by subtracting the spectra of the corresponding tin-free zeolites and normalised by the tin content in the materials. The amount of tin species with tetrahedral coordination geometry was calculated as  $KM_{210\text{ nm}} / (KM_{210\text{ nm}} + KM_{230\text{ nm}} + KM_{250\text{ nm}})$  and the loss of tetrahedral tin sites ( $T_d$  loss) was estimated based on the ratio between the value obtained for the fresh and the used samples. Diffuse-reflectance Fourier transform infrared (DRIFT) spectroscopy was performed using a Bruker Optics Vertex 70 spectrometer equipped with a high-temperature DRIFT cell (Harrick) and an MCT detector. Spectra were recorded in the range of 4000–400 cm<sup>-1</sup> under a N<sub>2</sub>

flow and at 473 K by co-addition of 200 scans with a resolution of 4 cm<sup>-1</sup>. Prior to the measurements, the samples were dried at 673 K under a N<sub>2</sub> flow for 4 h. The amount of carbon present in the catalysts after reaction was determined by elemental analysis using a LECO CHN-9000 instrument. To examine the tin distribution within the zeolite crystal, the powder samples were embedded in a resin (LR White Medium grade) and thin cross sections (*ca.* 90 nm thick) were prepared with a microtome (Ultra-cut S, Leica). Scanning transmission electron micrographs (STEM) in bright field (BF) and high-angle annular dark field (HAADF) modes as well as energy dispersive X-ray spectroscopy (EDS) element maps were acquired on a FEI Talos instrument operated at 200 kV. HAADF images were collected before and after EDS measurements to corroborate the absence of morphological changes.

### Catalytic testing

**Batch experiments.** Batch catalytic experiments were carried out under autogenous pressure in 15 cm<sup>3</sup> thick-walled glass vials (Ace, pressure tubes, front seal) dipped in an oil bath heated at 383 K. The vials were loaded with *ca.* 10 ml of a 0.33 M aqueous or methanolic solution of DHA (Merck, 98%) or PAL (Acros Organics, 40%) or a 0.33 M aqueous solution of D-xylose (Sigma-Aldrich, >99%). Then, the appropriate amount of catalyst was added to achieve a substrate/tin molar ratio of 1000. The mixture was allowed to react under vigorous stirring for 15 min. Then, the reaction was quenched using an ice bath and the catalyst removed by means of a Chromafil Xtra 0.25  $\mu$ m syringe filter. The turnover frequency (TOF) was calculated based on the mole of product formed per time and per mole of Sn. The conversion was limited to 40% in DHA and PAL isomerisation and to 15% in XYLO isomerisation in order to derive reliable initial rates.

**Continuous experiments.** Catalytic tests were performed using a homemade continuous-flow reactor setup (Fig. 1) comprising (i) an HPLC pump (Gilson-306), (ii) a stainless steel

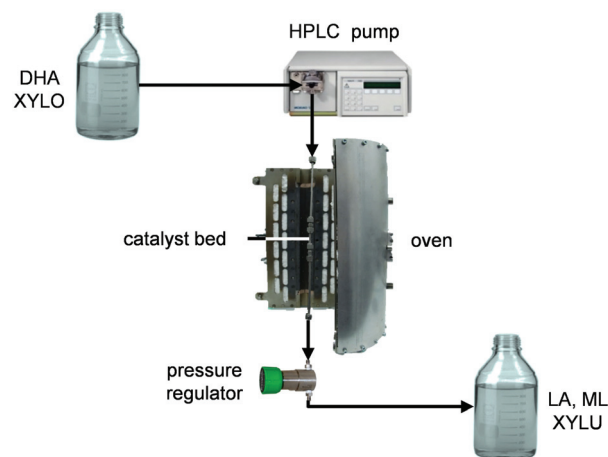


Fig. 1 Continuous-flow fixed-bed reactor used in this study.

tubular reactor with a precolumn (Swagelok SS-T4-S-035, o.d. = 1/4 inch, i.d. = 4.6 mm), both heated in a tubular oven and (iii) a backpressure regulator (Swagelok, LH2981001). The reactor was loaded with the catalyst (0.05–0.25 g), diluted with quartz (0.3–1.0 g, sieve fraction = 0.25–0.36 mm), and inserted into a tubular oven heated at 383 K. Thereafter, a liquid feed (0.2 cm<sup>3</sup> min<sup>-1</sup>, 0.33 M DHA/H<sub>2</sub>O and XYLO/H<sub>2</sub>O or 0.4 cm<sup>3</sup> min<sup>-1</sup>, 0.33 M DHA/MeOH) was added. To prevent evaporation of the solvent at the reaction temperature, the system was pressurised to 25 bar prior to heating. Samples were periodically collected at the outlet of the reactor. To better compare the extent of deactivation for the various samples, the ratios between TOF or selectivity at the time of interest and the corresponding values after 1 h on stream are presented. Absolute data for initial conversion and selectivity are compiled in Tables S1–S3 in the ESI.†

**Reaction analysis.** DHA, PAL, LA and glyceraldehyde (GAL) were isolated by high-performance liquid chromatography (HPLC) in a Merck LaChrom system equipped with a Biorad Aminex HPX-87H column heated at 308 K and a refractive index detector (Hitachi Chromaster model 5450) set at 303 K, using sulphuric acid (0.005 M, 0.6 cm<sup>3</sup> min<sup>-1</sup>) as the eluent. XYLO, XYLU and LYX were analysed in the same system using a Biorad Aminex HPX-87C column heated at 353 K and water (0.45 cm<sup>3</sup> min<sup>-1</sup>) as the eluent. Quantification was attained based on the absolute peak areas. ML was analysed using a gas chromatograph (HP 6890) equipped with an HP-5 capillary column and a flame ionisation detector. Quantification was accomplished by integration of its peak using iso-octane (Fluka, 99.5%) as an internal standard. Calibration curves were measured in the 0.1–10 wt% range using DHA, PAL, GAL (Sigma-Aldrich, >90%), L-lactic acid (ABCR, 98%), ML (TCI, >98%), XYLO and LYX (ABCR, 99%). In the case of XYLU, the response factor obtained for XYLO was used. The conversion of the substrate was calculated as the number of moles of the substrate reacted divided by the number of moles of the substrate fed, and the product yield as the number of moles of the product formed divided by the initial number of moles of the

substrate. The conversion of the substrate  $i$  ( $X_i$ ) and selectivity to the product  $k$  ( $S_k$ ) were calculated as:

$$X_i = 1 - (n_{i,1}/n_{i,0})$$

$$S_k = n_{k,1}/(n_{i,0} - n_{i,1})$$

where  $n$  refers to the moles of  $i$  or  $k$  and 0/1 to the reaction beginning/end.

The carbon balance was calculated as the ratio between the moles of products and the moles of reactant and was higher than 95% both in batch and in continuous experiments. The experimental error, determined by three repetitions of selected runs, was within 3%. No conversion of  $i$  was observed in blank tests.

## Results and discussion

### Preparation of tin-containing MFI, BEA, MOR and FAU zeolites

Tin-containing zeolites featuring distinct framework topologies were prepared *via* hydrothermal synthesis and/or alkaline-assisted metallation of commercial high-silica materials. MFI-type samples comprised zeolites crystallised in the presence of OH<sup>-</sup> or F<sup>-</sup> ions ([Sn]MFI-OH and [Sn]MFI-F) and stannated silicalite-1 (original bulk Si/Al = 1000, Sn-MFI). Since the two mineralising agents are known to lead to crystals with different size and amount of surface defects,<sup>5b</sup> the former solids enable a comparison of the effect of hydrophobicity on the catalytic performance. Analysis by XRD confirmed the typical MFI pattern for all of the materials. The crystallinity of Sn-MFI was *ca.* 30% lower in comparison with the parent silicalite, in line with earlier reports.<sup>5b</sup> The textural properties of all zeolites were in agreement with previous evidence (Table 1). The lower BET and mesoporous surface area of [Sn]MFI-F compared to [Sn]MFI-OH are related to its bigger particle size. In the case of Sn-MFI, the inferior microporous volume and BET area with respect to the parent zeolite are attributed to the loss of crystallinity upon stannation, while the higher mesoporous

**Table 1** Characterisation data of the tin-containing zeolites

Catalyst	Sn content <sup>a</sup> (wt%)	V <sub>pore</sub> <sup>b</sup> (cm <sup>3</sup> g <sup>-1</sup> )	V <sub>micro</sub> <sup>c</sup> (cm <sup>3</sup> g <sup>-1</sup> )	S <sub>meso</sub> <sup>c</sup> (m <sup>2</sup> g <sup>-1</sup> )	S <sub>BET</sub> <sup>d</sup> (m <sup>2</sup> g <sup>-1</sup> )
MFI	0.00	0.19	0.14	45	317
MOR	0.00	0.23	0.20	15	450
BEA	0.00	0.31	0.18	122	472
FAU	0.00	0.45	0.30	117	693
[Sn]MFI-OH	1.39	0.21	0.17	26	464
[Sn]MFI-F	0.90	0.18	0.14	6	335
Sn-MFI	1.87	0.29	0.08	98	246
Sn-MOR	1.65	0.31	0.17	43	499
[Sn]BEA-F	1.40	0.29	0.20	16	527
Sn-BEA	1.71	0.40	0.13	115	375
Sn-FAU	1.72	0.51	0.26	71	783

<sup>a</sup> ICP-OES. <sup>b</sup> Volume adsorbed at  $P/P_0 = 0.99$ . <sup>c</sup>  $t$ -Plot method. <sup>d</sup> BET method.

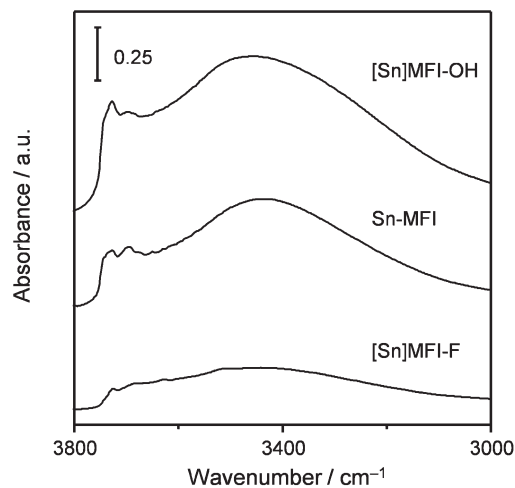


Fig. 2 DRIFT spectra of the tin-containing MFI zeolites.

area is due to the concomitant generation of mesopores in the post-synthetic treatment.<sup>16</sup> The presence of defects in the MFI zeolites was studied by DRIFT spectroscopy (Fig. 2). For all of the samples, two narrow bands at 3750 and 3695  $\text{cm}^{-1}$  attributed to terminal and internal silanol groups, respectively, and a broad band with maximum at *ca.* 3400  $\text{cm}^{-1}$ , assigned to hydrogen-bonded hydroxyls in nests, were evidenced.<sup>17</sup> These absorptions were intense for [Sn]MFI-OH and Sn-MFI and much weaker for [Sn]MFI-F, corroborating a hydrophilic character for the former two zeolites and a more hydrophobic nature for the latter.

Tin-containing BEA zeolites included a solid prepared by a seeded hydrothermal protocol,<sup>14</sup> which exhibited analogous textural properties to the literature benchmark, and a stannated BEA (original bulk Si/Al ratio = 220). Alkaline-assisted metallation was conducted in the presence of tetrapropylammonium ( $\text{TPA}^+$ ) ions, since these species have been shown to minimise the dissolution of the zeolite.<sup>15</sup> XRD indicated that *ca.* 45% of the initial crystallinity was lost. In line with this, the microporous volume and BET surface area of the Sn-BEA sample were smaller with respect to the parent BEA. Similarly to the case of Sn-MFI, mesoporosity was enhanced upon stannation.

The top-down method was applied to generate tin-containing MOR and FAU zeolites, which cannot be attained by bottom-up approaches. No major alteration in the textural properties of the original MOR zeolite (bulk Si/Al = 110) was observed, except for a slight increase in the mesoporosity. The decrease in crystallinity (–10%) and micropore volume determined upon metallation of FAU (bulk Si/Al = 405) was also moderate. As for the BEA framework,  $\text{TPA}^+$  was added upon modification to protect this zeolite from excessive amorphisation.<sup>15</sup> Elemental analysis indicated a tin content of 0.9–1.9 wt % in the solids (Table 1).

The characterisation of the coordinative environment and of the Lewis acidity of the tin centres was performed by diffuse-reflectance UV-Vis spectroscopy and infrared spectroscopy of adsorbed  $\text{d}_3$ -acetonitrile. Two main contributions

at *ca.* 210 and 230 nm were observed in the UV-Vis spectra of the samples (Fig. 3a), indicative of tetra- and hexacoordinated Sn(IV) species present in the zeolite framework and at the extra framework positions, respectively. An additional minor band was detected at 250 nm, which is attributed to polymeric  $\text{SnO}_2$  species.<sup>18</sup> Framework tin is commonly accepted as the catalytically active centre in the reactions of interest, as demonstrated by the negligible product yields determined over tin oxide.<sup>11</sup> The relative intensity of the bands associated with these two species varies significantly between the different samples. In the case of MFI zeolites, the amount of tetra-coordinated Sn centres is slightly higher than that of the hexacoordinated sites for [Sn]MFI-F and Sn-MFI, but the latter is predominant in [Sn]MFI-OH. In the case of the BEA zeolites, the metallated material features a higher proportion of tetra-coordinated species compared to the hydrothermally-prepared sample. For Sn-MOR and Sn-FAU, most of the tin centres possess a tetrahedral geometry. The FTIR spectra of adsorbed  $\text{d}_3$ -acetonitrile evidenced a band located at *ca.* 2310  $\text{cm}^{-1}$  and attributed to the stretching vibration of the nitrile group bound to tetrahedral tin sites for all solids (Fig. 3b). Concerning the MFI, MOR and FAU materials, the position of this band is the same, indicating a similar strength of the acid centres, while its intensity, proportional to the density of sites, follows the same trend as indicated by the UV-Vis spectroscopy analysis. For the BEA zeolites, the FTIR spectra point to a higher amount of Lewis-acid sites in [Sn]BEA-F than in Sn-BEA, in contrast to the UV-Vis spectroscopy results. Furthermore, the blue-shift of the band (2313 *vs.* 2308  $\text{cm}^{-1}$ ) highlights a higher acid strength for the tin sites in the hydrothermally-prepared zeolite. This discrepancy could originate from the distinct spatial sensitivity of the UV-Vis and FTIR spectroscopic techniques applied, *i.e.*, surface and bulk, respectively. Accordingly, the former overestimates the fraction of tin oxide present in [Sn]BEA-F, which is typically located at the surface of the crystals, and is likely blind to extra framework tin sites situated in the intracrystalline mesopores of Sn-BEA.

### Catalytic activity

The tin-containing catalysts were initially tested in the batch conversion of PAL into LA or ML using water or methanol as the solvent, respectively, to determine their intrinsic activities. PAL was chosen as the substrate instead of DHA in order to ensure a comparison of the materials exclusively based on their Lewis-acidic properties. Indeed, the transformation of PAL only comprises a 1,2-hydride shift within its hemihydrate or hemiacetal, while that of DHA first involves a Brønsted-acid catalysed dehydration to PAL (Scheme 1).<sup>19</sup> The TOF values determined in the aqueous tests (Fig. 4a) generally indicate the following order of framework-based activity: BEA > FAU > MFI > MOR, where Sn-BEA falls slightly out of the trend. Since the relative amount of tetrahedral tin sites evidenced by spectroscopic characterisation does not fit this trend (Fig. 3), this result points to a dominant role of the geometry of the tin site,<sup>20</sup> where centres located in larger channels seem more suitable. Still, the superior mass transfer properties of large/3D

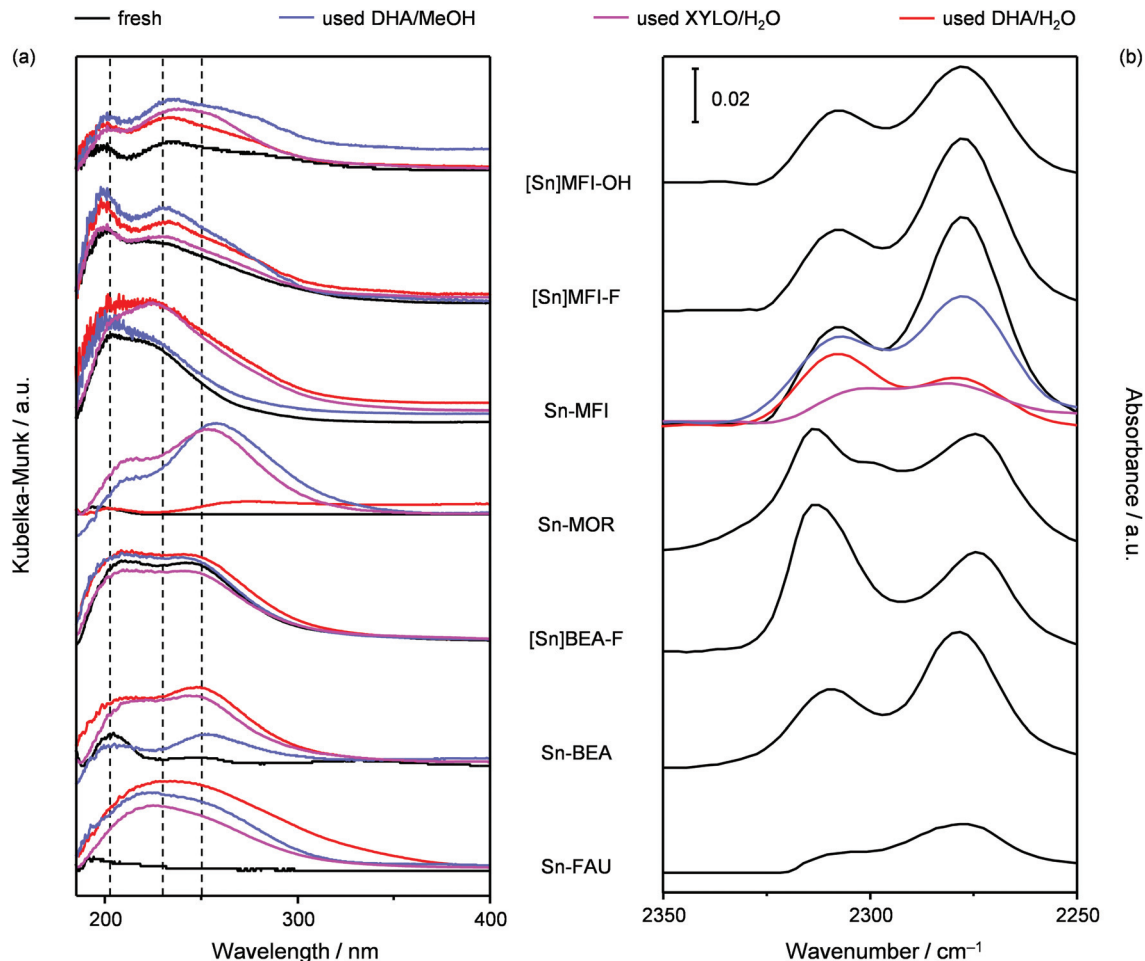


Fig. 3 (a) UV-Vis spectra and (b) FTIR spectra of adsorbed  $d_3$ -acetonitrile of the tin-containing zeolites.

compared to medium/1D pore structures might be relevant too. When considering the same framework but a different preparation method, metallated zeolites were less active than their hydrothermally-synthesised counterparts, suggesting that the advantage of a greater mesoporosity is surpassed by the drawback of a lower amount of framework tin (Fig. 3). In contrast, taking into account the similar content in tetracoordinated tin centres and its higher hydrophobicity, the inferior activity of [Sn]MFI-F with respect to [Sn]MFI-OH might arise from the larger crystal size. The tests performed with methanol as the solvent evidenced a comparable framework-based ranking (Fig. 4b). Still, the activity of the zeolites characterised by 12-membered rings (BEA and FAU) almost doubled compared to that observed in water (*e.g.*, 2700 vs. 1300  $\text{h}^{-1}$  for [Sn]BEA-F), while, for zeolites with 10-membered rings (MFI), the activity in methanol was *ca.* 1.5 times lower. The former evidence might be explained based on the lower polarity of an alcoholic than aqueous medium, which affects to a more limited extent the Lewis acidity of the sites, while the latter finding may be due to the prevailing effect of mass transport phenomena. In this respect, the bulkier methanol-solvated

methyl lactate is likely to encounter more diffusion constraints with respect to the water-solvated lactic acid. This speculation seems supported by the TOF of Sn-MOR, which, despite featuring large pores, is more prone to diffusion issues due to their monodimensionality.

Although the conversion of PAL represents a useful test reaction for the determination of the Lewis sites activity for the 1,2-hydride shift, the transformation of DHA possesses a higher industrial potential, being this substrate obtainable by chemo- or biocatalytic oxidation of glycerol in high yields.<sup>21</sup> Upon evaluating its conversion in water, most of the catalysts displayed a similar TOF (Fig. 4c), indicating a lower dependence of this reaction on the framework and quality of the tin centre compared to PAL. This could be ascribed to the fact that, at this temperature, the dehydration step to PAL is rate limiting, as already suggested.<sup>19</sup> Since the best performing materials were the hydrophobic [Sn]MFI-F and [Sn]BEA-F, we hypothesise that the lower interaction of water with the zeolite surface favours the shifting of the dehydration equilibrium towards the PAL intermediate.<sup>22</sup> The same solvent effect was observed as for the conversion of PAL, that is, the activity of

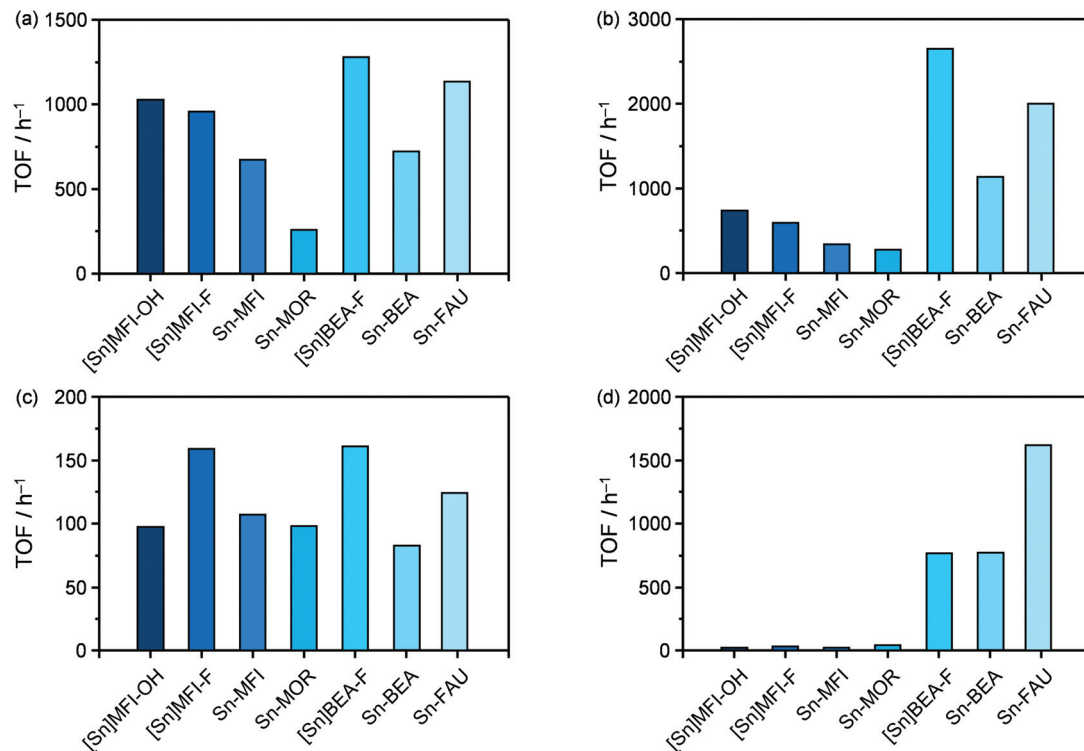


Fig. 4 Turnover frequency of the tin-containing zeolites in the isomerisation of PAL in (a) water or (b) methanol and of DHA in (c) water or (d) methanol.

zeolites featuring smaller or less interconnected pores was lower than that of the materials with larger pores when methanol was used as the medium (Fig. 4d).

In view of the relevance of sugar isomerisation, we also assessed the activity of the tin-containing zeolites in the conversion of XYLO into XYLU. This pentose was preferred to the hexose glucose since the latter does not fit in purely microporous MFI zeolites, thus excluding these materials from the comparison. The TOF data (Fig. 5) generally indicate a slower reaction rate with respect to the isomerisation of PAL, which

can be ascribed to the bigger size of the substrate compared to the trioses. Specifically, strong diffusion limitations seemed to affect the reaction over MFI zeolites. The fact that the TOF over Sn-MOR is not at the same level as in the isomerisation of PAL and DHA suggests a more critical effect of pore size compared to pore connectivity. Considering catalysts with the same topology, the performances appeared to be mostly influenced by the quality of the tin centres, as exemplified by the TOF of the metallated and the respective hydrothermally-prepared materials. The surprisingly low TOF measured for Sn-FAU might relate to the more pronounced stability issues associated with this sample, as discussed hereon.

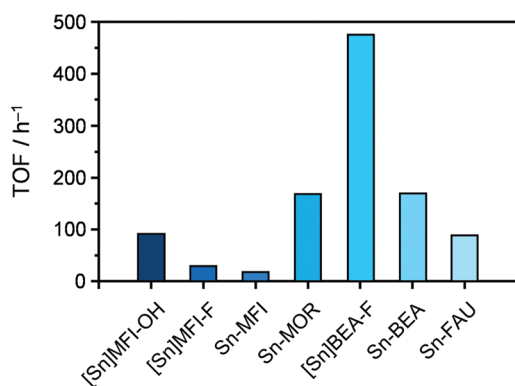


Fig. 5 Turnover frequency of the tin-containing zeolites in the isomerisation of XYLO in water.

### Stability under continuous-flow operation

The stability of the tin-containing zeolites was studied under continuous operation in a fixed-bed reactor for 24 h during DHA and XYLO isomerisation in the same media as for the batch investigations. Upon the aqueous conversion of DHA, all of the materials showed marked deactivation (50 to 100% activity loss, Fig. 6a and b). The most stable sample was Sn-MFI, which preserved about half of the original performance level and displayed almost constant selectivity (Fig. S1 in the ESI†), while the TOF dropped by 80% over hydrothermally-prepared MFI and BEA zeolites, and Sn-FAU, Sn-MOR and Sn-BEA became almost inactive. In all cases, the depletion of activity was accompanied by a more or less pronounced reduction of the selectivity. In order to understand the origin of the

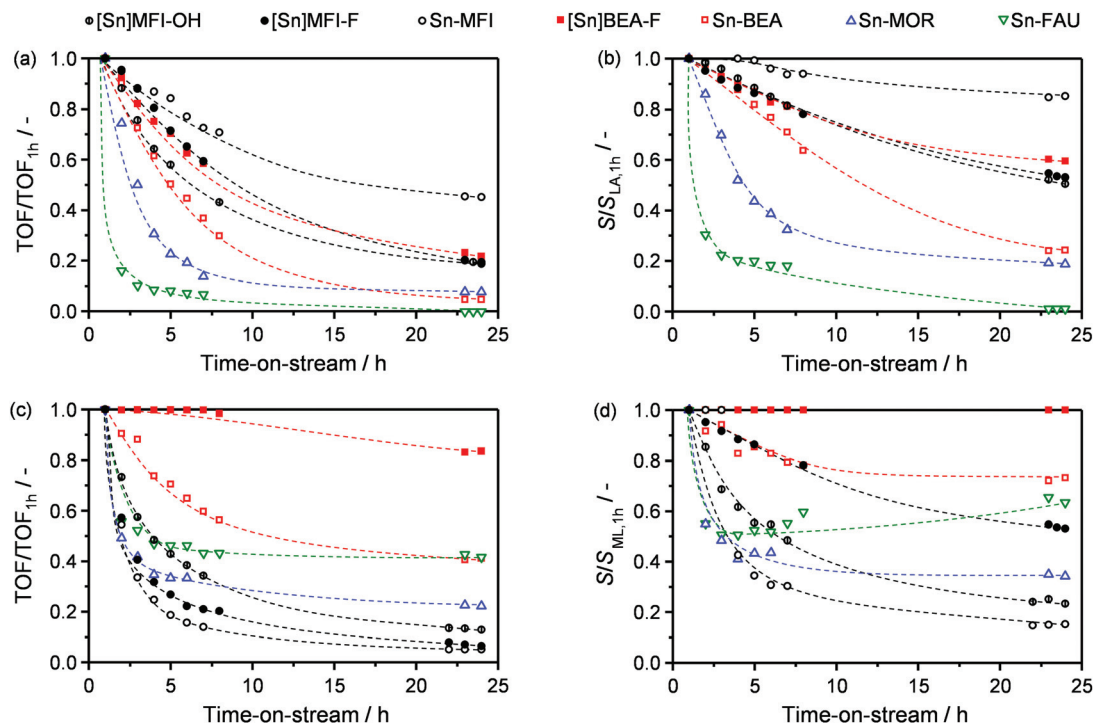


Fig. 6 Fraction of initial activity and of initial selectivity to LA for the tin-containing zeolites in the isomerisation of DHA in water (a, b) or in methanol (c, d).

Table 2 Characterisation data of the tin-containing zeolites after the continuous-flow tests

Catalyst	Reaction	Sn loss <sup>a</sup> (%)	Crystallinity loss <sup>b</sup> (%)	Carbon content (wt%)	T <sub>d</sub> loss <sup>c</sup> (%)
[Sn]MFI-OH	DHA/H <sub>2</sub> O	0	0	1.2	36.8
	DHA/MeOH	0	0	2.9	41.2
	XYLO/H <sub>2</sub> O	21	29	0.7	50.8
[Sn]MFI-F	DHA/H <sub>2</sub> O	2	0	3.8	15.7
	DHA/MeOH	5	0	1.9	1.7
	XYLO/H <sub>2</sub> O	5	7	0.5	0.4
Sn-MFI	DHA/H <sub>2</sub> O	0	41	1.0	20.0
	DHA/MeOH	15	2	5.4	-4.7
	XYLO/H <sub>2</sub> O	17	19	0.6	29.2
Sn-MOR	DHA/H <sub>2</sub> O	1	0	2.7	33.3
	DHA/MeOH	0	17	1.2	71.8
	XYLO/H <sub>2</sub> O	5	47	1.8	66.7
[Sn]BEA-F	DHA/H <sub>2</sub> O	0	18	0.4	1.3
	DHA/MeOH	4	0	1.1	8.1
	XYLO/H <sub>2</sub> O	0	3	4.3	0.2
Sn-BEA	DHA/H <sub>2</sub> O	10	13	0.7	65.3
	DHA/MeOH	46	28	3.7	59.8
Sn-FAU	XYLO/H <sub>2</sub> O	53	6	1.8	63.7
	DHA/H <sub>2</sub> O	0	100	0.7	63.6
	DHA/MeOH	1	51	1.3	64.3
	XYLO/H <sub>2</sub> O	0	45	1.4	60.5

<sup>a</sup> ICP-OES. <sup>b</sup> XRD. <sup>c</sup> UV-Vis.

observed deactivation, the used catalysts were studied by UV-Vis spectroscopy, elemental analysis and XRD (Fig. 3a and Table 2). For the MFI stannosilicates, the characterisation data indicate that the tin content was preserved but the tetrahedral

sites significantly restructured into inactive hexacoordinated species. For Sn-MFI substantial amorphisation of the zeolite took place, in contrast to [Sn]MFI-OH and [Sn]MFI-F, which fully retained their crystallinity. The presence of higher carbon

content in these materials after the reaction suggests that their greater loss in activity compared to Sn-MFI was related to the irreversible adsorption of carbonaceous species especially on the sites that are responsible for the formation of LA, therefore causing both a diminished activity and selectivity (Fig. S1 in the ESI†). In the case of zeolites featuring the BEA framework, considering the negligible changes to the tin properties and content, the moderate decrease in crystallinity stands as the dominant reason for the performance loss of [Sn]BEA-F, while partial amorphisation, tin leaching and restructuring contributed to the deactivation of Sn-BEA. The more extensive degradation of Sn-BEA might be due to the smaller crystal size, *i.e.*, higher surface to volume ratio, the higher hydrophilicity and the larger content of surface defects. For Sn-MOR, heavy modification in the coordination of the active sites occurred and coke formed to a significant extent. The latter presumably was more detrimental for the accessibility of the tin sites for this catalyst than for the MFI stannosilicates, owing to the monodimensional pore network. The extremely rapid deactivation of Sn-FAU, accompanied by a strong loss in selectivity, was ascribed to a remarkable modification of the tin centres and to the total loss of crystallinity, which is in line with the poor hydrothermal stability of USY zeolites.<sup>10a</sup> In order to determine whether the substrate, the product or the aqueous solvent provoked the change in the structure of the active sites, Sn-BEA was exposed to water and aqueous solutions of DHA and LA under reaction-like conditions. The UV-Vis spectra of the catalyst retrieved after 15 and 60 min of these batch treatments indicated a similarly strong alteration of the tin sites, pointing to water as being mainly responsible for their coordinative changes (Fig. 7).

When methanol was used as the medium for DHA isomerisation, the deactivation extent of the zeolites was overall

similar to the previous case (55 to 95%) with the exception of Sn-BEA, which showed only a moderate (12%) loss of activity (Fig. 6c and d). On the other hand, the framework-related trend was reversed: MFI zeolites were the worst catalysts followed by MOR and then FAU and BEA, which converged to the same level of functionality. Again, both activity and selectivity were suppressed, as highlighted in the case of Sn-MFI (Fig. S2 in the ESI†). Considering MFI materials, the crystallinity was fully retained, but the tin species underwent a change in coordination, although to a lower degree than in the aqueous test, and appreciable tin loss was observed for both [Sn]MFI-F and Sn-MFI. Additionally, equivalent amounts of carbon were deposited on these samples.

Regarding [Sn]BEA-F, a slight tin loss and coke deposition were evidenced, but both the zeolitic structure and the tin geometry were unaltered, which is in line with the minor decrease in activity and the retention of the selectivity. Conversely, Sn-BEA showed significantly reduced crystallinity, a clear increase of hexacoordinated tin sites and fouling. Additionally, half of the tin contained in this sample was leached out. The similarly performing Sn-FAU suffered equivalent alteration of the coordination of tin and fouling and an even greater loss in crystallinity, but minimal leaching of the active metal. An equivalent scenario was characterised for Sn-MOR after the methanol-based test, although the better preservation of the zeolitic framework was surpassed by a more significant conversion of tetrahedral tin into octahedral tin. Overall, the use of methanol compared to that of water hindered the structural alterations of the zeolites and the extent of modification in the coordination of the active centres. However, tin leaching was more pronounced. This result is quite surprising, since amorphisation and tin expulsion from the framework appear as phenomena which favour leaching and they were more relevant in water. We therefore supposed that leaching in the aqueous medium remained somehow undetected. In this respect, based on the inorganic chemistry of tin ions in water at variable pH,<sup>23</sup> we put forward that tin cations leached in the aqueous reaction mixture (minimum pH of 3.83) readily hydrolyse into hydroxide species which are insoluble and are retained in the catalytic bed. In contrast, tin ions leached in methanol are soluble in this medium and are flushed away. This hypothesis was further corroborated by adding SnCl<sub>4</sub> to methanol and water and observing a clear solution in the first case, while the formation of a suspended white precipitate in the second. Finally, we considered the conversion of XYLO into XYLU in water. Based on the stronger chelating properties of this substrate compared to DHA, this alternative isomerisation is interesting to further elucidate the role of highly-functionalised biobased species in deactivation processes. The catalytic data indicate minor performance loss for [Sn]MFI-OH, and a depletion of the original functionality by 20, 40, 75 and 92% for [Sn]MFI-F and [Sn]BEA-F, Sn-MFI and Sn-MOR, Sn-BEA and Sn-FAU, respectively (Fig. 8a). As in the previous cases, hydrothermally-prepared samples were more stable than stannated catalysts. As observed in the conversion of DHA in water, pronounced modification of the tin structure and deterioration of

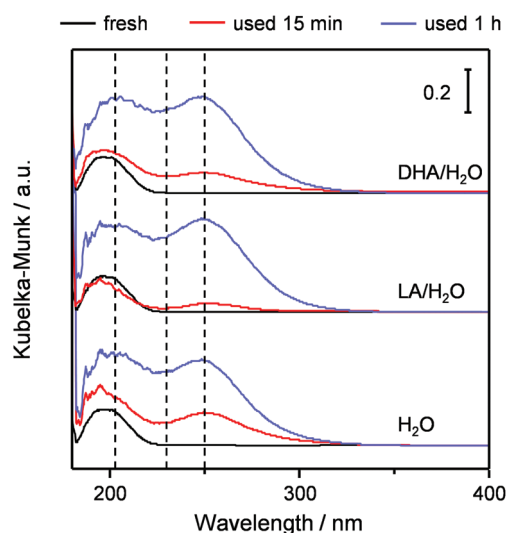


Fig. 7 UV-Vis spectra of Sn-BEA after exposure to water and to aqueous solutions of DHA and LA under reaction-like conditions in batch mode.

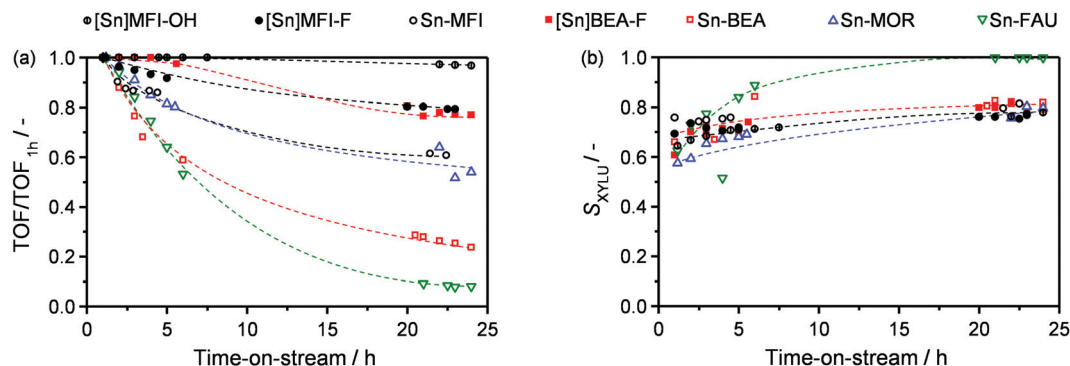


Fig. 8 (a) Fraction of initial activity and (b) XYLU selectivity for the tin-containing zeolites in the isomerisation of XYLO in water.

the crystallinity were identified. Yet, the presence of the sugar substrate/product also led to greatly enhanced tin leaching and fouling. In view of the ligand-properties of the reactant and product, leached tin species might be stabilised in water prior to hydrolysis and precipitation and flushed away, in contrast to the case in which DHA was processed. Carbohydrates are also known to be a source of the by-product and polymeric species, which are irreversibly adsorbed and cause coking. In spite of the activity loss, the selectivity of all the materials slightly increased with time on stream (Fig. 8b and S3 in the ESI†). This can be explained by the fact that, at progressively lower conversion levels, XYLU is formed in lower amounts and therefore the rate of its reaction to LYX is diminished. The full selectivity to XYLU observed in the case of Sn-FAU at the end of the run is a consequence of the LYX concentration being below the detection limit of the HPLC analysis.

### Characterisation of used Sn-MFI

Sn-MFI was selected for a deeper characterisation after the continuous reactions. Changes in the coordination of the tin centres were further investigated by FTIR of adsorbed  $d_3$ -acetonitrile. In agreement with the data obtained by UV-Vis spectroscopy, the intensity of the acetonitrile band at  $2310\text{ cm}^{-1}$ , attributed to sites with tetrahedral geometry, was reduced in the samples retrieved from the aqueous phase tests (Fig. 3b). This was more pronounced in the case of the material used in XYLO isomerisation since, in addition to the restructuring of the tin sites, leaching also occurred (Table 2). After the reaction in methanol, the amount of active sites was only slightly diminished, confirming that the strong deactivation observed was almost fully attributable to fouling. The only slightly inferior DHA conversion measured after 1 h on stream during

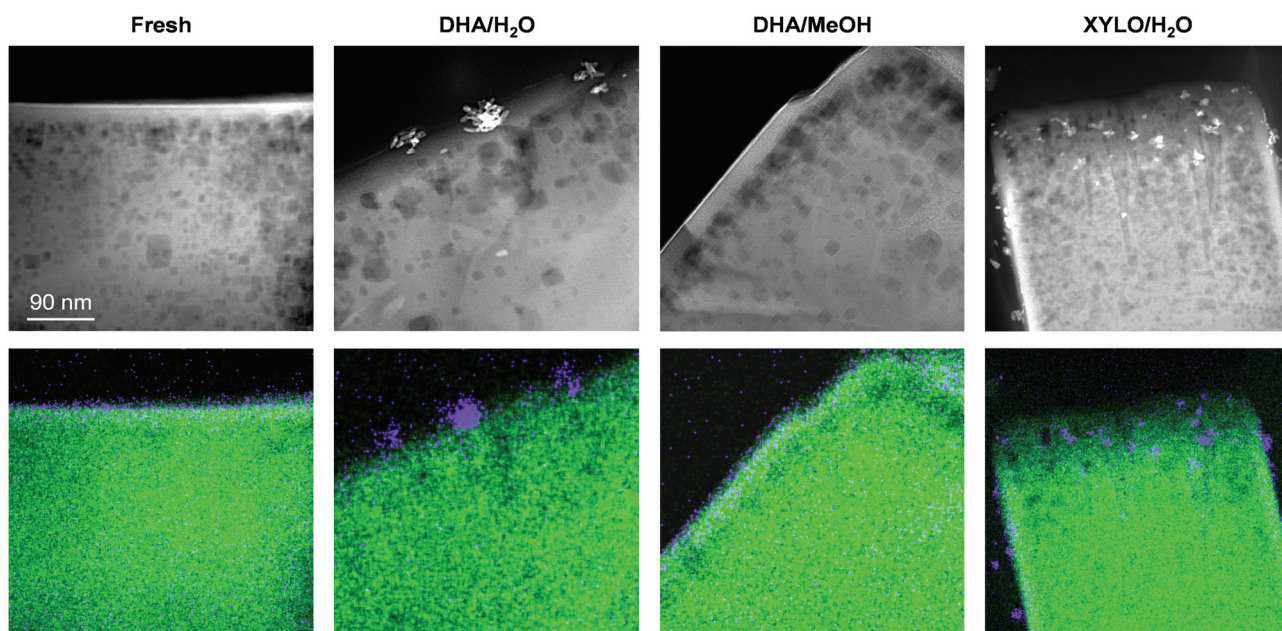


Fig. 9 HAADF-STEM images (top-row) and corresponding chemical maps (bottom row) of thin cross sections of Sn-MFI before and after the continuous flow tests. In the EDS maps, green corresponds to silicon ( $K\alpha$ ) and purple to Sn ( $L\alpha$ ).

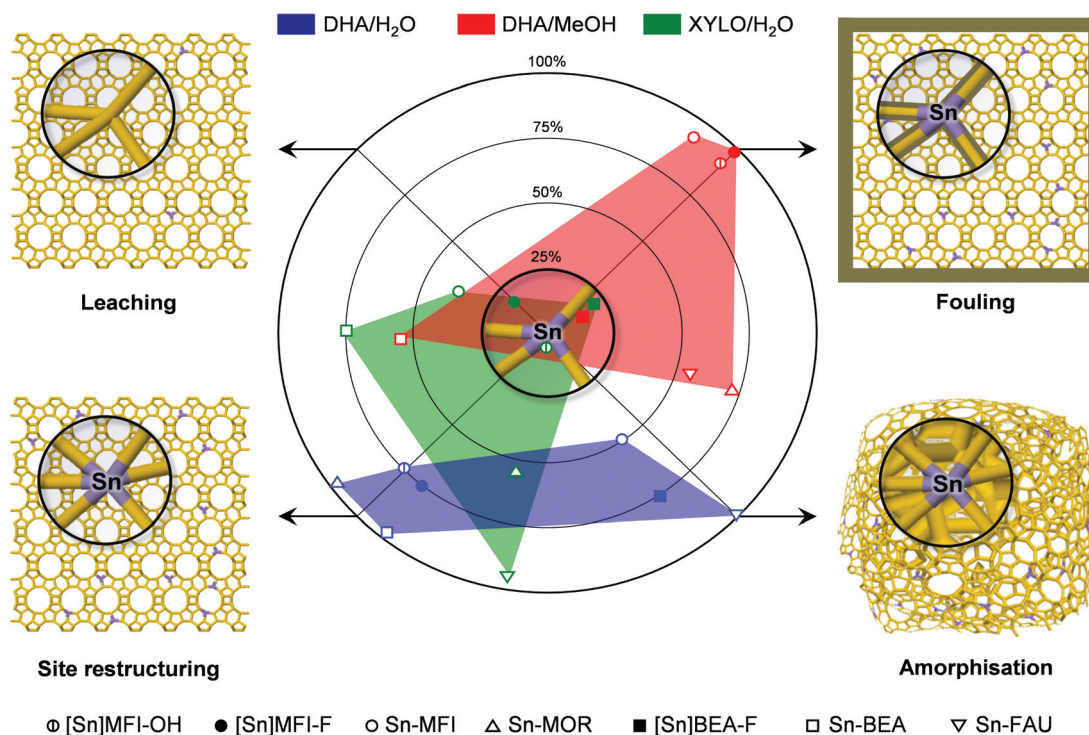
a new test over the used catalyst after regeneration by calcination strongly supports this finding (Table S2 in the ESI†).

Modifications to the location and morphology of tin within the zeolite crystals could be clearly visualised by microscopy examination of thin cross sections (Fig. 9). In agreement with the enhanced accessibility expected for Lewis sites introduced by alkali-assisted stannation,<sup>16</sup> HAADF-STEM images and chemical maps of the fresh catalyst reveal that the Sn centres are concentrated close to the external surface of the MFI crystal and are highly dispersed (*i.e.*, no extra framework tin oxide nanoparticles are detected). The crystal itself exhibits well-defined edges and intracrystalline mesopores that develop concurrently during the metallation treatment. Comparatively, significant alteration of the metal dispersion was observed following application for DHA or XYLO conversion in water, after which the tin is mainly seen to be located in oxidic tin nanoparticles decorating the external surface of the zeolites, although a few nanoparticles are observed to form within the zeolite mesopores. Consistent with the increased leaching evidenced due to substrate chelation in the transformation of XYLO with respect to DHA, the nanoparticles appear smaller (*ca.* 4–8 nm compared to 10–15 nm in diameter) and more uniformly distributed in the catalyst applied for the former. Moreover, in line with the substantial amorphisation of the zeolite in the conversion of DHA, the outer surface of the crystal looks significantly eroded. A similar, but less prominent effect was

observed after the conversion of XYLO. In stark contrast, the appearance of the sample used in methanol closely resembles that of the fresh catalyst, with no obvious evidence of tin redistribution, nanoparticle formation or structural changes of the zeolite. These findings nicely corroborate the expected deactivation mechanisms in each of the reaction systems.

## Conclusions

In this study, we have confronted tin-containing MFI, MOR, BEA and FAU zeolites obtained by hydrothermal synthesis and post-synthetic stannation in alkaline media in the isomerisation of dihydroxyacetone in water and methanol and in that of xylose in water, evaluating their activity in batch mode and their stability under industrially-relevant conditions, *i.e.*, under continuous operation in a fixed-bed reactor. The turn-over frequencies of the BEA and FAU stannosilicates were greater than those of the MFI and MOR materials in the aqueous tests and increased and decreased, respectively, in the methanol-based experiments, evidencing a framework-specific interplay between the structural and mass transfer properties. Hydrothermally-prepared MFI and BEA zeolites were more active than their metallated counterparts owing to the higher quality of the tin sites and greater hydrophobicity. The continuous tests uncovered a moderate to dramatic deactivation of



**Scheme 2** Overview of the extent and type of deactivation in the tin-containing zeolites after the continuous experiments. The distance of the points from the middle circle, identifying reasonable stability and preservation of the original features of the tin centres, indicates the degree of deactivation, expressed in the range from 0 to 100%. Each point is located between the two main mechanisms of deactivation at an angular position that is inversely proportional to the weight of each.

the catalysts. In particular, we found that, if the solvent is water, both the activity and selectivity are lost primarily due to the amorphisation of the zeolite framework and the degradation of the active tin centres (Scheme 2), which are displaced to extra framework positions and/or completely leached from the solid to the reaction medium. These drawbacks were minimised using methanol as the solvent, although, in this case, fouling led to a significant deactivation of MFI zeolites and tin leaching was higher. This is a promising result in view of a prospective industrialisation of these materials, since a process based on this alcoholic medium is associated with higher sustainability and lower cost. In the case of sugars such as xylose, which can be handled only in aqueous media due to solubility issues, hydrothermally-prepared [Sn]MFI and [Sn]BEA-F were identified as the best candidates to attain stable operation. Deactivation mechanisms in this transformation were similar to those in the case of the aqueous isomerisation of dihydroxyacetone, but the chelating properties of the sugars and the irreversible adsorption of side and polymerisation products enhanced tin loss and fouling.

## Acknowledgements

This work was supported by the Swiss National Science Foundation (Project Number 200020-159760). A. J. Saadun is acknowledged for experimental input.

## References

- R. Rinaldi and F. Schüth, *Energy Environ. Sci.*, 2009, **2**, 610.
- E. Taarning, C. M. Osmundsen, X. Yang, B. Voss, S. I. Andersen and C. H. Christensen, *Energy Environ. Sci.*, 2011, **4**, 793.
- (a) M. Moliner, *Dalton Trans.*, 2014, **43**, 4197; (b) J. Dijkmans, D. Gabriels, M. Dusselier, F. de Clippel, P. Vanelderden, K. Houthoofd, A. Malfliet, Y. Pontikes and B. F. Sels, *Green Chem.*, 2013, **15**, 2777; (c) P. Wolf, C. Hammond, S. Conrad and I. Hermans, *Dalton Trans.*, 2014, **43**, 4514; (d) C. M. Osmundsen, M. S. Holm, S. Dahl and E. Taarning, *Proc. R. Soc. London, Ser. A*, 2012, **468**, 2000.
- P. Y. Dapsens, C. Mondelli and J. Pérez-Ramírez, *Chem. Soc. Rev.*, 2015, **44**, 7025.
- (a) C. Hammond, S. Conrad and I. Hermans, *Angew. Chem., Int. Ed.*, 2012, **51**, 11736; (b) P. Y. Dapsens, C. Mondelli, J. Jagielski, R. Hauert and J. Pérez-Ramírez, *Catal. Sci. Technol.*, 2014, **4**, 2302.
- M. Morales, P. Y. Dapsens, I. Giovinazzo, J. Witte, C. Mondelli, S. Papadokonstantakis, K. Hungerbühler and J. Pérez-Ramírez, *Energy Environ. Sci.*, 2015, **8**, 558.
- (a) P. Y. Dapsens, C. Mondelli and J. Pérez-Ramírez, *ACS Catal.*, 2012, **2**, 1487; (b) J.-P. Lange, *Angew. Chem., Int. Ed.*, 2015, **54**, 13186.
- Y. Román-Leshkov and M. E. Davis, *ACS Catal.*, 2011, **1**, 1566.
- I. Sádaba, M. López Granados, A. Riisager and E. Taarning, *Green Chem.*, 2015, **17**, 4133.
- (a) R. M. Ravenelle, F. Schuessler, A. D'Amico, N. Danilina, J. A. van Bokhoven, J. A. Lercher, C. W. Jones and C. Sievers, *J. Phys. Chem. C*, 2010, **114**, 19582; (b) D. W. Gardner, J. Huo, T. C. Hoff, R. L. Johnson, B. H. Shanks and J.-P. Tessonier, *ACS Catal.*, 2015, **5**, 4418; (c) L. Zhang, K. Chen, B. Chen, J. L. White and D. E. Resasco, *J. Am. Chem. Soc.*, 2015, **137**, 11810.
- (a) M. Moliner, Y. Román-Leshkov and M. E. Davis, *Proc. Natl. Acad. Sci. U. S. A.*, 2010, **107**, 6164; (b) N. Rajabbeigi, A. I. Torres, C. M. Lew, B. Elyassi, L. Ren, Z. Wang, H. J. Cho, W. Fan, P. Daoutidis and M. Tsapatsis, *Chem. Eng. Sci.*, 2014, **116**, 235.
- (a) J. D. Lewis, S. Van de Vyver, A. J. Crisci, W. R. Gunther, V. K. Michaelis, R. G. Griffin and Y. Román-Leshkov, *ChemSusChem*, 2014, **7**, 2255; (b) S. Van de Vyver, C. Odermatt, K. Romero, T. Prasomsri and Y. Román-Leshkov, *ACS Catal.*, 2015, **5**, 972.
- N. K. Mal, V. Ramaswamy, P. R. Rajamohan and A. V. Ramaswamy, *Microporous Mater.*, 1997, **12**, 331.
- S. Valencia and A. Corma, *US Pat*, 5968473, 1999.
- (a) D. Verboekend, G. Vilé and J. Pérez-Ramírez, *Adv. Funct. Mater.*, 2012, **22**, 916; (b) P. Y. Dapsens, C. Mondelli and J. Pérez-Ramírez, *New J. Chem.*, 2012, DOI: 10.1039/C5NJ01834J.
- P. Y. Dapsens, C. Mondelli, B. Kusema, R. Verel and J. Pérez-Ramírez, *Green Chem.*, 2014, **16**, 1176.
- P. Wu, T. Komatsu and T. Yashima, *J. Phys. Chem.*, 1995, **99**, 10923.
- R. Bermejo-Deval, R. Gounder and M. E. Davis, *ACS Catal.*, 2012, **2**, 2705.
- F. de Clippel, M. Dusselier, R. Van Rompaey, P. Vanelderden, J. Dijkmans, E. Makshina, L. Giebel, S. Oswald, G. V. Baron, J. F. M. Denayer, P. P. Pescarmona, P. A. Jacobs and B. F. Sels, *J. Am. Chem. Soc.*, 2012, **134**, 10089.
- G. Li, E. Pidko and E. J. M. Hensen, *Catal. Sci. Technol.*, 2014, **4**, 2241.
- (a) G. M. Lari, C. Mondelli and J. Pérez-Ramírez, *ACS Catal.*, 2015, **5**, 1453; (b) D. Hekmat, R. Bauer and J. Fricke, *Bioprocess Biosyst. Eng.*, 2003, **26**, 109; (c) H. Kimura, K. Tsuto, T. Wakisaka, Y. Kazumi and Y. Inaya, *Appl. Catal., A*, 1993, **96**, 217.
- P. Li, G. Liu, H. Wu, Y. Liu, J. Jiang and P. Wu, *J. Phys. Chem. C*, 2011, **115**, 3663.
- C. I. House and G. H. Kelsall, *Electrochim. Acta*, 1984, **29**, 1459.